

17. S. Harrington, "Prices and profits in the liability insurance market" (paper presented at the Brookings Institution Conference on Legal Liability, Washington, DC, 15 June 1987).
18. J. Greenwald, *Business Insurance*, vol. 1 (10 February 1986).
19. On-Line Reports, Best's Review, Property/Casualty Insurance Edition (A. M. Best, Oldwick, NJ, February 1985).
20. For views at the poles, compare Insurance Services Office, in (22) and Insurance Services Office, "Insurer profitability: A long-term perspective" (New York, NY, 1987), with National Insurance Consumer Organization, "And now the real facts: A response to the Insurance Services Office's 'Insurer Profitability: The facts'" (Alexandria, VA, undated).
21. G. Gottheimer, in *Crisis Avoidance: Insurance Responsibilities*, N. Williams, Ed. (Society of Chartered Property & Casualty Underwriters, Malvern, PA, 1986).
22. Insurance Services Office, "Insurer profitability—the facts" (New York, NY, February 1986); Insurance Services Office, "1985, a critical year: A study of the property-casualty insurance industry" (National Association of Independent Insurers, New York, NY, May 1985).
23. R. Hunter, "Taming the latest insurance 'crisis,'" *New York Times* (13 April 1986), p. F3; "The manufactured crisis: Liability-insurance companies have created a crisis and dumped it on you," *Consumer Reports* (August 1986), p. 544.
24. For example, B. Stewart, in *Issues in Insurance*, J. Long, Ed. (American Institute for Property and Liability Underwriters, Malvern, PA, 1981), vol. 2, p. 79.
25. Some studies have suggested that the cycle timing and amplitude may vary by line, for example, Conning & Company, "A study of why underwriting cycles occur" (Hartford, CT, 1979).
26. R. McGee, *Fed. Reserve Bank NY Q. Rev.* 11, 22 (Autumn 1986).
27. E. Venezian, "Ratemaking methods and profit cycles in property and liability insurance," *J. Risk Insurance* 52, 477 (September 1985).
28. Munch and Smallwood, *Bell J. Econ.* 11, 261 (Spring 1980); J. Finsinger and M. Pauly, in *Risk and Capital*, G. Bamber and K. Spremann, Eds. (Springer-Verlag, New York, 1983).
29. New York Governor's Advisory Commission on Liability Insurance, "Insuring our future" (Albany, NY, 7 April 1986).
30. P. M. Danzon, "The frequency and severity of medical malpractice claims" (Rand, Santa Monica, CA, 1982).
31. Alliance of American Insurers, American Insurance Association, National Association of Independent Insurers, "Property and casualty insurance industry data and the case for tort reform" (Schaumburg, IL, June 1986).
32. I am indebted to B. Mathew for excellent research assistance in the preparation of this article.

The Use of a Charge-Coupled Device for Quantitative Optical Microscopy of Biological Structures

YASUSHI HIRAOKA, JOHN W. SEDAT, DAVID A. AGARD

The properties of a charge-coupled device (CCD) and its application to the high-resolution analysis of biological structures by optical microscopy are described. The CCD, with its high resolution, high sensitivity, wide dynamic range, photometric accuracy, and geometric stability, can provide data of such high quality that quantitative analysis on two- and three-dimensional microscopic images is possible. For example, the three-dimensional imaging properties of an epifluorescence microscope have been quantitatively determined with the CCD. This description of the imaging properties of the microscope, and the high-quality image data provided by the CCD, allow sophisticated computational image processing methods to be used that greatly improve the effective resolution obtainable for biological structures. Image processing techniques revealed fine substructures in *Drosophila* embryonic diploid chromosomes in two and three dimensions. The same approach can be extended to structures as small as yeast chromosomes or to other problems in structural cell biology.

OPTICAL MICROSCOPY (OM) IS A POWERFUL YET STILL underexploited approach for analyzing biological structure and function at the cellular level. Biological specimens can be examined in an aqueous, defined ionic environment under nonperturbing conditions and in many cases in the living state. Also, OM techniques are extremely rapid and permit many samples to be

examined under a wide variety of conditions. Especially since the advent of specific probes such as monoclonal antibodies, cloned DNA sequences, DNA-specific dyes, and calcium and pH-dependent fluorophores (1, 2), cellular organization can be explored with high selectivity. Large cells, specific tissues, or, as in the case of *Caenorhabditis elegans* (3), whole organisms can be analyzed by OM.

Although biological samples are intrinsically three-dimensional, traditional OM methods have provided only a two-dimensional (2-D) representation of the three-dimensional (3-D) organization; also, the analysis is generally not quantitative. To overcome these limitations, we have been developing 3-D data collection methods for OM in conjunction with powerful image-processing techniques (4–6) to examine biological structures at the cellular level. We investigated the 3-D organization of interphase chromosomes initially with *Drosophila melanogaster* polytene chromosomes as a model system (4, 6–8). Optical section data in digital format was computationally processed (6) to remove the out-of-focus information that contaminated each image plane. The resultant 3-D image was analyzed by computer-aided modeling to reveal the spatial arrangements of the chromosomes within the nucleus (9, 10). This was followed by an analysis of the 3-D structures (6–8) as a function of transcription patterns, cell type, and developmental stage.

We recently extended these studies to the high-resolution analysis of *D. melanogaster* embryonic diploid chromosomes, which have a nuclear diameter that is 1/10 that of the polytene chromosomes. To reconstruct a 3-D image at a resolution approaching the diffraction limit of an optical system, it is critical that the out-of-focus

The authors are at the Department of Biochemistry and Biophysics and the Howard Hughes Medical Institute Structural Biology Unit, University of California San Francisco, San Francisco, CA 94143-0448.

information be removed. The success of this process strongly depends on the numerical accuracy of the microscopic data; thus high-resolution 3-D imaging data must be both photometrically and geometrically accurate. This article describes the imaging characteristics of the charge-coupled device (CCD) and its use as an ideal imaging tool for high-resolution 3-D OM. We also show that CCD image data are of sufficient quality to allow experimental determination of the imaging properties of an epifluorescence microscope.

The CCD is a relatively new device for image detection; functionally it is equivalent to electronic film. These devices were originally developed for military use and have now become available for scientific applications including astronomy (11, 12). Most recently, Connor reported the application of a CCD for Ca^{2+} imaging (13). Throughout this article we use the term CCD to refer only to high-quality scientific imagers that are capable of directly integrating the image on the chip; we do not consider the CCDs in home video cameras that are simply low-cost alternatives to vidicon cameras. To take full advantages of the CCD for high-resolution analysis, we characterized the optical properties of the cooled CCD.

This article documents the properties of the CCD for image detection in OM. This detector combines high resolution, high sensitivity, extraordinarily wide dynamic range, photometric accuracy, and geometric stability, all of which are required for the image processing. Figure 1 schematically illustrates how the CCD produces an image. The CCD imager is a solid-state detector with a metal-oxide-semiconductor structure (11, 12) that ensures geometric fidelity. When a CCD is exposed to light, electron-hole pairs are generated within the semiconductor at a high quantum efficiency; the electrons then accumulate in an electric potential well at each pixel (picture element). The electron-hole pairs are generated in

direct proportion to the incident photons and thus provide an extremely linear response (11). The accumulated electrons are transferred from one well to another (Fig. 1B) to a readout amplifier (12) in a process called "charge-coupling." The charge-coupling transfer technique does not require separate readout wires to each pixel so that high resolution can be achieved by placing a very large number of pixels in a rather compact area. Chips that range up to 2048 by 2048 pixels can be obtained (each pixel is between $6\ \mu\text{m}$ and $27\ \mu\text{m}$ square). The quantum efficiency of some CCDs is extremely high (20 to 70%) in the 350- to 1000-nm wavelength range that is often used in optical microscopy, as compared with an efficiency of 10 to 20% for a conventional photomultiplier detector (12).

System Description

Our OM system is built around a Zeiss inverted Axiomat microscope that was modified so that stage, focus, and data collection are fully computer controlled (4, 9). A CCD camera made by Photometrics (Tucson, Arizona) that consists of a dewar for liquid nitrogen cooling and associated electronics was attached to the straight-through port of the Axiomat. Conventional relay optics are used to couple the microscope to the CCD camera. The entire microscope system is isolated from vibration. The CCD consists of a buried channel, thinned, back-illuminated 1024 by 640 pixel chip (16 mm by 10 mm active area; RCA Inc.). The thinned chip provides increased sensitivity in blue light (14). This particular chip has a full-well depth of about 300,000 electrons and a readout noise of less than 50 electrons. The CCD is kept at $-120^\circ \pm 0.1^\circ\text{C}$ by temperature regulation to eliminate thermal generation of electrons

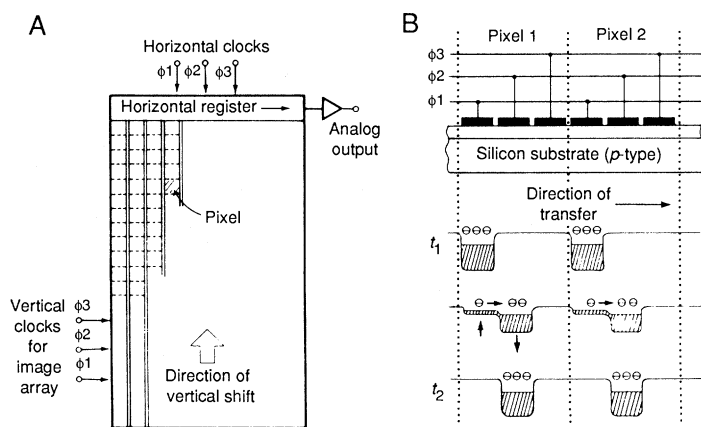


Fig. 1. (A) CCD architecture and (B) the charge-transfer mechanism in a three-phase CCD. The CCD chip is composed of a series of columns and rows (separated by vertical solid lines and horizontal broken lines, respectively) to produce an array of pixels; the hatched square represents one pixel. Each column is insulated from the others; a "blooming" drain is located between columns to remove excess electrons from saturated areas and prevents vertical smearing of the image, or "blooming," under intense illumination. An amplifier at the top of the chip provides the electron signal readout in the form of an analog voltage; other electronic circuits convert this analog signal into digital values. Upon exposure to light, electrons are captured and accumulate in a potential well generated in each pixel. The CCD can integrate signals until the potential well becomes full of electrons. After exposure an entire row of accumulated electrons are transferred along each column into the horizontal register followed by a horizontal transfer to be read out. This sequence repeats one row after another until all the pixels are read out. The charge transfer, both vertical and horizontal, proceeds as potentials are sequentially clocked by three-phase pulses (designated ϕ_1, ϕ_2 , and ϕ_3); correspondingly, each pixel has a set of three electrodes. The diagram illustrates only a single step that pushed electrons from one electrode to the next (adapted with permission from Photometrics, Tucson, Arizona).

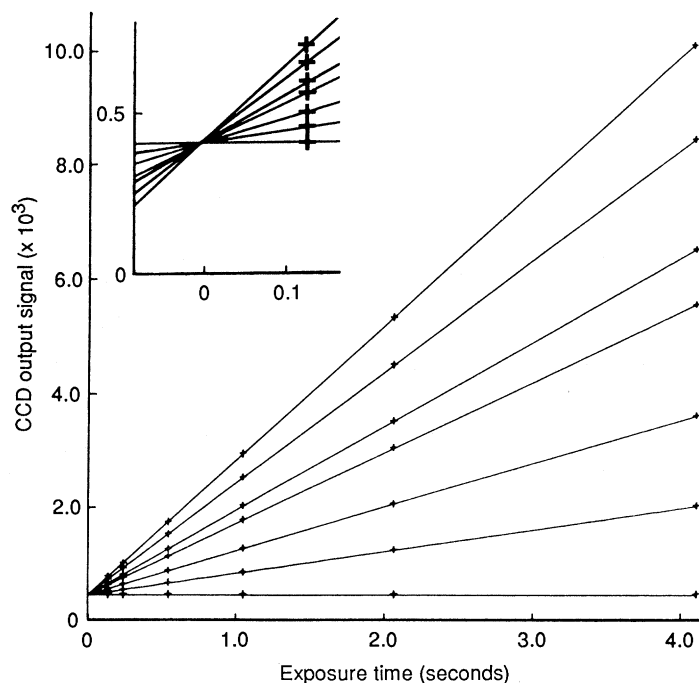


Fig. 2. Linear response of CCD. Six blank-field images were taken on the CCD at exponentially increasing exposure times under constant and uniform 405-nm illumination. The average pixel intensity was plotted as a function of exposure time. A set of these plots obtained at various light levels is shown with lines calculated by least-squares as a function of time. The linearity result was obtained over the entire dynamic range of the CCD. The horizontal line shows the no illumination output signal (dark current); all the other lines extrapolate to this baseline at essentially a single offset value (shown in inset), indicating the invariance of pixel characteristics with illumination level.

within each pixel. The thermal electrons decrease approximately tenfold for every 20°C drop in temperature and are essentially eliminated below -90°C, which allows exposure times of up to several hours. The output signals of the CCD are digitized by the Photometrics camera controller to a resolution of 14 bits per pixel (16,384 gray levels) and are transferred at 50,000 pixels per second to a bulk memory system (Texas Memory Systems) and then stored and analyzed in a VAX 11/780 computer system (15). The optical resolution element (pixel) size is 16 μm in the image plane, which corresponds to 60 nm in the object plane for a 63 \times objective lens or 38 nm for 100 \times objective lens. Thus the image resolution is not limited by the pixel resolution.

Properties of the CCD System in Optical Microscopy

We initially characterized the CCD system by illuminating the detector through the microscope under the same conditions normal-

ly used to obtain OM data but with essentially uniform blank fields. Image fields were taken on the CCD for a series of exposure times at a constant light intensity. The average pixel intensity was plotted as a function of exposure time and repeated at various illumination levels (Fig. 2). The response linearity of each pixel was monitored by analysis of the deviations from a least-squares line and for pixels that were considered to be problematic (16); values at those locations were replaced by the average value of surrounding pixels. Linearity was obtained over the range of wavelengths commonly used in optical microscopy (17). The importance of linearity is that the absolute intensity of a microscopic image or object can be obtained from the output signals of the CCD.

A CCD picture of a uniformly illuminated field is in fact nonuniform because of pixel variations in gain (sensitivity) and offset (baseline) (Fig. 3A). The high linearity of the CCD facilitates correction of these pixel variations by a simple linear algorithm. A correction file that contained both gain and offset values for each pixel was made by a pixel-by-pixel linear regression analysis from six uniform image fields that were integrated for different times. Pixel variations present in the raw image were almost completely removed in the corrected image (Fig. 3, A and B), with the standard deviation being reduced from 90 to 24 with a mean gray level of 3150 (full scale of 16,384). It is not necessarily easy to tell from a single picture if there are subtle correction problems. Pixel variations, if any, can be more clearly seen in an edge view of several pictures of the same image taken in succession and stacked together (Fig. 3, C and D). In the x - z plane-edge view, for example, vertical lines represent pixels that have not been completely corrected; the resultant systematic variations are readily distinguished from statistical noise.

Fourier transformation analysis can also be used to illustrate systematic problems in images acquired from various imaging

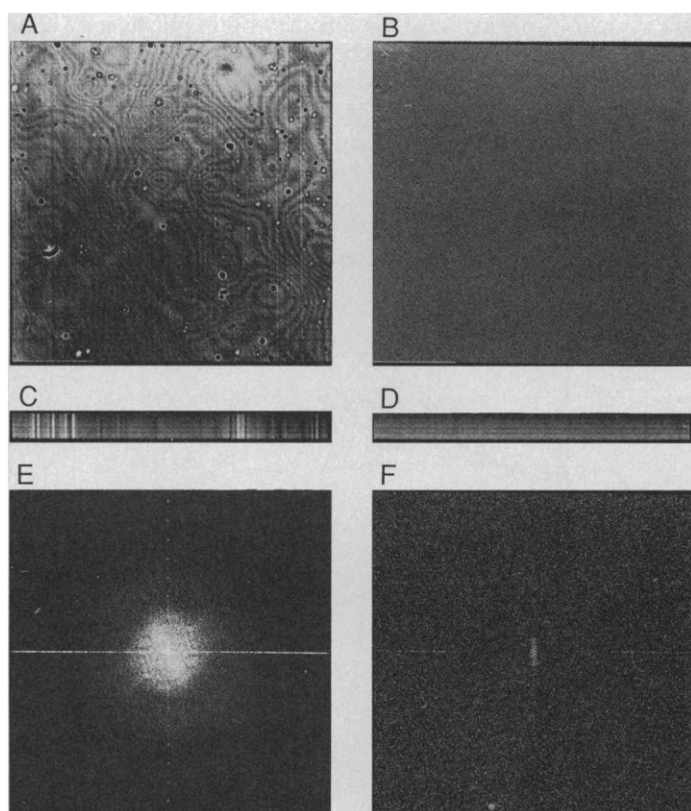


Fig. 3. Field uniformity of a CCD image. A correction file that contains gain and offset values for each pixel was made from several brighter uniform images taken at exponentially increasing exposure times as described in Fig. 2 and from one dark-field image. The extrapolated offset obtained in this way is not identical to the dark-field image in spite of its extrapolation to the baseline value. Unlike the extrapolated offset, the dark-field image did not remove the pixel variations completely, especially those characteristic of each column. A raw image (A) is displayed at 256-level gray level mapping that corresponds to image values of 3,000 to 3,300 (full scale of 16,384). The corrected image at (B) of 2,600 to 2,900. The interference pattern seen in the raw image is typical of highly monochromatic illumination. Edge views of a stacked image are shown for the uncorrected (C) and corrected (D) data, respectively. The bright or dark vertical lines, which represent systematic pixel variations, are present in (C) and removed in (D). In (E) and (F), 2-D Fourier transforms of the raw and corrected images are shown [the scale is expanded ten times in (F)]. The bright line that starts at the lower left corner (where the readout amplifier is located) is due to an electronic problem that was not properly eliminated by an early version of the decalibration software.

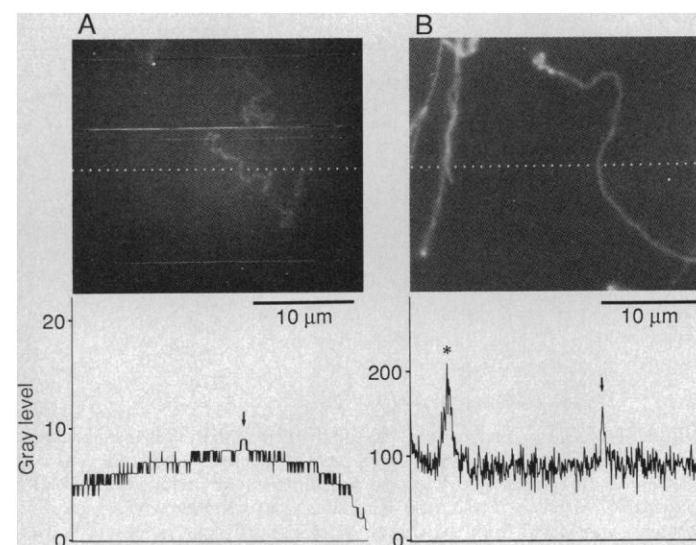


Fig. 4. Comparison of SIT and CCD image quality. Phenol-extracted bacteriophage T4 DNA molecules were stained with 0.1 $\mu\text{g}/\text{ml}$ DAPI in 1 mM sodium cacodylate, 10 mM MgCl_2 , and 1% 2-mercaptoethanol (15) and examined with a Zeiss Neofluar 100 \times [numerical aperture (NA) = 1.3] oil immersion objective lens. A 365-nm band pass (BP) exciter filter, a 395-nm dichroic mirror and a combination of a 395-nm long wave pass (LP) filter and a 560-nm short wave pass (SP) filter as a barrier filter, as was done for all of the DAPI-stained chromosome studies presented in this article. The SIT (A) and CCD (B) images are displayed at gray level mappings of 0 to 40 and 0 to 400, respectively; a plot of the gray scale along the horizontal dotted line is shown (single DNA molecule is located at an arrow; a peak indicated by an asterisk in (B) corresponds to a bundle of two DNA molecules). The magnification of the SIT image is 1.06 times greater than that of the CCD image.

devices. Systematic noise or distortion in the image can produce characteristic spots or intensity distributions in the transform (18). Fourier transformation of CCD images before and after correction are shown in Fig. 3, E and F. The power spectrum of the corrected image consists mainly of a central peak at zero spatial frequency (Fig. 3F is shown at a scale that is expanded ten times compared with Fig. 3E). Thus by its uniformity the Fourier transform result also documents the absence of systematic problems with CCD image acquisition. By contrast, errors in video camera data are often seen by this method.

Although the observed field nonuniformity (Fig. 3A) is dominated by the CCD pixel characteristics, there are subtle optical effects that depend on both objective lens and wavelength. For this reason all of the images described below in this article were adjusted with a correction file made under standardized conditions at or near focus for each objective lens and at each wavelength (19).

One of the intrinsic properties of a CCD is its ability to directly integrate photons as electrons at a high quantum efficiency during exposure. This means that in principle the CCD can be used to count photons. In practice, it is possible to generate high-quality images under very low light. In Fig. 4 the image quality of the CCD is compared with that of the silicon-intensified target (SIT) camera, a nonintegrating television (TV) device. Single DNA molecules stained with the DNA-specific dye 4',6-diamidino-2-phenylindole (DAPI) (20) were imaged. The SIT camera image was digitally averaged for 256 frames (8.5 seconds). The CCD image is the result of an 8-second integration. To facilitate comparison of image quality, gray level information along a horizontal line is shown in Fig. 4. The position of the DNA molecule is shown by an arrow. Comparison of the DNA signal with background noise in both devices indicates that the CCD is superior to the SIT camera in terms of signal-to-noise ratio. Thus the CCD is capable of accurately obtaining extremely weak image information.

Optical Characterization of a Microscope System

The optical parameters for a microscope are best described in terms of either the direct-space point-spread function (PSF) or the reciprocal-space contrast-transfer function (CTF). The PSF describes how a point image spreads by passage through the optical system; the CTF is the Fourier transform of the PSF.

Our approach to determining the PSF of the microscope was to directly image single fluorescent beads with a diameter of 0.1 μm . Since this is smaller in size than the resolution limit, they effectively behave as point objects. Polystyrene beads coated with a fluorescent dye that emits light at 450 nm (similar to the emission spectrum of DAPI, which was used in most of our biological experiments) were dried onto glass slides and imaged in a glycerol medium to match the refractive index. This was done both in focus and at many positions above and below the focal plane. The PSF was analyzed for several objective lenses. Typically we collected 33 images that each differed by 0.25 μm in the focus direction z (thus from $z = +4 \mu\text{m}$ to $z = -4 \mu\text{m}$). Several beads in each image were superimposed by a least-squares procedure after scaling the individual bead intensities (Fig. 5).

Analysis of the point images shows first that the images are in the form of a series of Airy rings and are strikingly asymmetrical about the focal plane. This asymmetry is especially severe with high numerical aperture (NA) lenses. Second, close inspection of the rings indicates that they are not circularly symmetric. An ideal optical system with a circular aperture should show circular symmetry for the rings and symmetry above and below the focal plane, as

predicted by diffraction optics theories (21, 22). Subsequent experiments indicated that the asymmetry of the images above and below the focal plane seen in all lenses tested (23) could be corrected by increasing or decreasing the refractive index of the immersion medium or by the use of objective lenses that had a correction collar to change the optical path length. As pointed out by Inoué, this result shows that residual spherical aberration is responsible for the focus asymmetry (24). The lack of circular symmetry and the ring substructure is specific to each objective lens; the patterns rotate exactly with rotation of the objective lens. It is likely that residual wave-front aberrations are responsible for this problem.

We calculated and radially averaged 2-D CTFs directly from the PSF images by 2-D Fourier transformation (Fig. 6). Inspection of the CTF plots shows that the in-focus curve has a gradual falloff to a high-frequency cutoff. The cutoff frequency, which provides an absolute measure of the resolution limit, was found to be about $(0.25 \mu\text{m})^{-1}$. Out-of-focus curves show a series of ripples and a rapid frequency falloff. Calculations that were based on known lens parameters and diffraction optics theory (21, 22) produced out-of-focus curves with ripples similar to those observed but that were slightly displaced. The total 3-D CTF was calculated from a stack of through-focus point images by a 3-D Fourier transformation (25).

Microscopic Image Improvement

As indicated above, a microscopic image is not an exact representation of the object but instead is distorted by passage through the optical system. In mathematical terms the observed image is a convolution of the true object with the PSF of the microscope (5, 18). To minimize the effects of microscopic aberrations it is necessary to deconvolute the observed images.

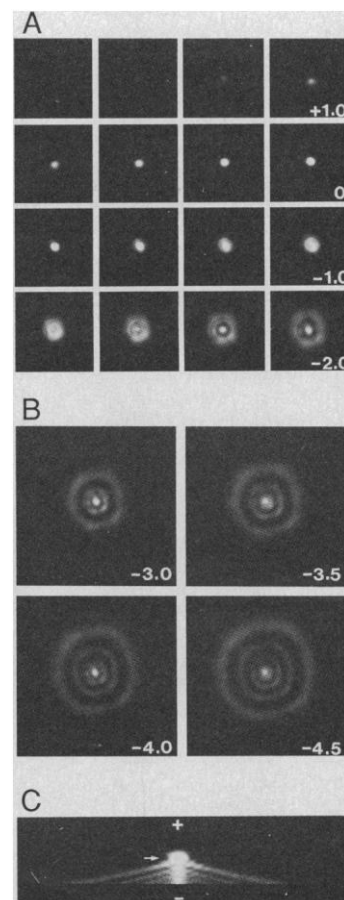


Fig. 5. Point images at defocus. Serial images of fluorescent microspheres (0.1- μm diameter; Pandex Laboratories, Inc.) were taken on the CCD by stepping the microscope focus by 0.25- μm intervals (**A** and **B**). This set of point images was obtained with a Leitz Planapo 63 \times (NA = 1.4) oil immersion objective lens on the Axiomat. A 405-nm BP exciter filter, 425-nm dichroic mirror and a combination of 425-nm LP and 560-nm SP barrier filter were used. The number in each panel is the amount of defocus in micrometers; the negative sign denotes the direction as the objective lens approaches the specimen. In (**A**) the point images, from +1.75 μm to -2.0 μm , are shown every 0.25 μm from left to right and top to bottom; -3.0, -3.5, -4.0, and -4.5 μm are shown in (**B**). The edge view of 3-D stack of 31 point images spanning from +3.0 μm to -4.5 μm with a 0.25- μm step size is shown in (**C**); the in-focus plane is shown by an arrow. All the images are displayed on a logarithmic scale to show a bright central peak and faint rings at the same time.

We used a thin, approximately 2-D biological sample to test the constrained deconvolution approaches with actual CCD image data. *Drosophila melanogaster* early embryos, stage 10 through 13, were squashed as described in Fig. 7. The corrected in-focus CCD images of early prophase chromosomes were deconvoluted by means of an iterative constrained method (5, 26) with the experimentally determined in-focus CTF described above. Figure 7 shows chromosome images before and after the resolution improvement. Strikingly detailed features can be seen in the deconvoluted images. The chromosomal substructure reveals $\sim 0.2\text{-}\mu\text{m}$ fibers that seem intertwined. Details of this substructure were directly substantiated by electron microscope tomographic analysis (27). Similar improvements have been obtained on a wide variety of biological specimens imaged under differing conditions. In general, we estimate that the Fourier cutoff resolution limit is improved from about $(0.25\ \mu\text{m})^{-1}$ to $(0.19\ \mu\text{m})^{-1}$. The important point is that quantitatively accurate images provided by the CCD are a starting point for computer enhancement that can dramatically improve the overall quality and resolution of images from biological samples.

We have extended these approaches to 3-D CCD image data. An intact whole *D. melanogaster* embryo prepared as described in Mitchison and Sedat (28) was used to obtain 3-D staged prophase nuclei under minimally perturbed conditions. Images from 24

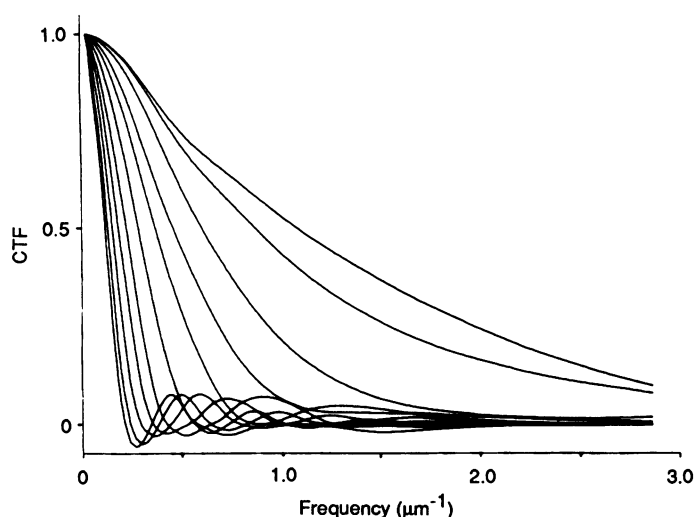
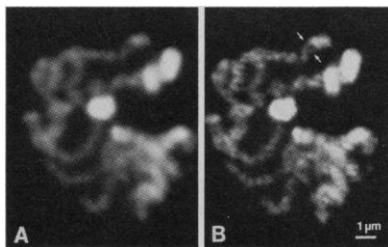


Fig. 6. Illustration of the 2-D contrast transfer function. Two-dimensional Fourier transforms were calculated from the point images shown in Fig. 5. The transform modulus was rotationally averaged; positive and negative signs were alternately given to the local maxima as expected from the transform of a point object.

Fig. 7. Resolution improvement of 2-D chromosome images. *Drosophila* early embryos were collected and squashed in buffer A (15 mM 1,4-piperazine-diethanesulfonic acid, pH 7, 80 mM KCl, 20 mM NaCl, 2 mM EGTA, 0.5 mM spermidine, 0.2 mM spermine, and 0.1% 2-mercaptoethanol) that contained 1% formaldehyde and 5 $\mu\text{g}/\text{ml}$ DAPI. A Leitz Planapo 63 \times (NA = 1.4) objective lens was used with oil immersion. (The same filters as described in Fig. 4 were used.) The image was processed by a constrained deconvolution algorithm (22) by using the in-focus CTF experimentally determined for the lens used; (A) is before and (B) is after. Intertwining fibers are indicated by arrows.



optical sections, each $0.5\ \mu\text{m}$ apart in z , were recorded on the CCD with a Zeiss 63 \times (NA = 1.2) cover slip-free water objective lens. Out-of-focus image contamination was removed by a simple algorithm (6) that approximates the more exact 3-D deconvolution approaches (5). Data from the planes above and below a given plane were used to calculate the out-of-focus contributions to the central plane. This blurring contribution was subtracted from the given plane and the process repeated for all planes. A late prophase nucleus in the embryo is shown in Fig. 8, before and after out-of-focus information removal. A much improved 3-D image results; after processing, we could identify centromeres, telomeres, and a helical feature (shown by an arrow) on the chromosome arms.

The same approach was applied to the yeast *Saccharomyces cerevisiae* (Fig. 9). A yeast cell nucleus showed a relatively uniform appearance after being stained with DAPI. The removal of out-of-focus information revealed unexpected substructures within the nuclear chromatin region. The chromosome-like rods seen in Fig. 9B had a diameter of $0.28\ \mu\text{m}$ and were similar to that of the *D. melanogaster* embryonic chromosomes in Fig. 8B and to those observed in the fission yeast *Schizosaccharomyces pombe* (29). The dimension of a yeast nucleus ($2\ \mu\text{m}$ in diameter) causes its image to be especially prone to both optical aberrations and out-of-focus image contamination in OM. Thus yeast chromosomes have been studied only in mitotically arrested cells in *S. pombe* (29, 30). The 3-D OM techniques that use the CCD could provide a powerful tool for analyzing *S. cerevisiae* as well as *S. pombe* chromosomes in a normal mitotic process.

Although the above method works satisfactorily, more exact methods such as full matrix or full 3-D Fourier deconvolution approaches that use an experimentally determined 3-D CTF, possibly in combination with tilting of the specimen (5), should result in higher resolution 3-D images.

Discussion

There has been much interest in TV image detection systems to replace photographic film for OM. Inoué (31) and Allen (32) have emphasized the amount of additional information that can be obtained by analog and digital manipulation of the TV image. The

Fig. 8. Optical sectioning of *Drosophila* embryonic chromosomes. Embryos were fixed with 3.7% formaldehyde and the coat and membrane were removed as described by Mitchison and Sedat (28). The embryos were stained with 0.1 $\mu\text{g}/\text{ml}$ DAPI and were attached by adhesion to a poly-L-lysine-coated glass slide and mounted in buffer A without a cover slip on the Axiomat. By using the Zeiss Planapochromat 63 \times (NA = 1.2) water immersion lens, serial pictures were taken on the CCD by stepping the microscope focus $0.5\ \mu\text{m}$ per step. The number in each panel represents the sequential order of the optical sections, each $1\ \mu\text{m}$ apart, from inside to outside of the embryo. Out-of-focus image contamination was removed by a simple nearest-neighbor algorithm (6); (A) is before and (B) is after processing. A helical feature in the chromosome arms is indicated by an arrow.

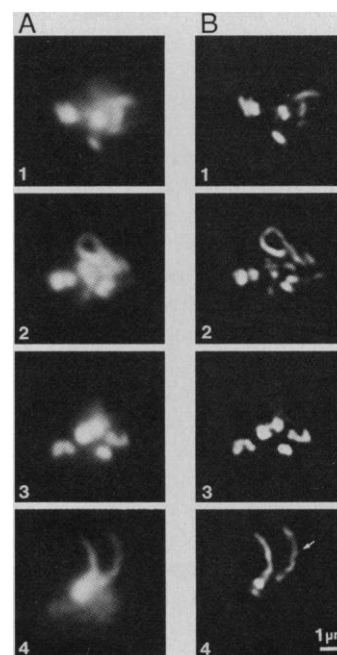
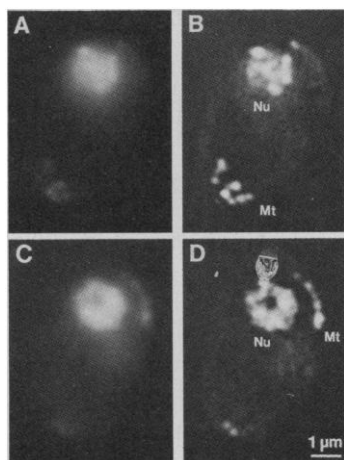


Fig. 9. Optical sectioning of the yeast *S. cerevisiae*. *Saccharomyces cerevisiae* cells were fixed with 3.7% formaldehyde, stained with 10 $\mu\text{g/ml}$ DAPI, and mounted in glycerol. By using the Leitz Planapo 63 \times (NA = 1.4) oil immersion lens on the Axiomat, 16 serial pictures were taken with a 0.25- μm focal increment. Two sections (A and B and C and D), each 1 μm apart, are shown; (A) and (C) are before and (B) and (D) are after processing. Abbreviations: Nu, nuclear chromatin region; Mt, mitochondria. The hole inside the nucleus in (D) is supposed to be the nucleolus.



SIT TV camera is perhaps the most widely used video camera because of its sensitivity, although the less sensitive but higher resolution Chalnicon or Newvicon tubes are generally used for differential interference contrast methods.

Unfortunately, even for general biological microscopy, video cameras are far from ideal detectors. TV cameras have a number of intrinsic problems, of which perhaps the most significant is the trade-off between resolution and sensitivity. In addition, the rather limited dynamic range of video cameras (approximately 6 to 7 bits) causes difficulties when attempting to visualize intense and weak information simultaneously, as in fluorescence microscopy. SIT camera images also tend to be extremely noisy, which is a problem that can only be partially overcome by digital averaging.

For quantitative or 3-D OM, the problems of conventional video cameras are even more severe. In 3-D OM the quantitative comparison of information from one image to another in a series of optical sections is required. One problem is that TV camera response is very nonlinear, which makes the determination of absolute intensities extraordinarily difficult. The situation is further exacerbated by geometric distortions that vary from one part of the field to another. In principle, if the various distortions could be determined, it should be possible to correct them digitally. However, TV systems are temporally unstable both in geometry and tube characteristics which makes it nearly impossible to correct the data adequately. Thus conventional video cameras can provide 3-D information only for low-resolution analysis in which numerical accuracy is not crucial.

We have shown that the CCD is an imaging device that can solve most of the problems intrinsic to low light level TV systems. Our data, as well as data of others (12), document that the CCD has a fixed geometry, very high sensitivity, extremely wide dynamic range, and high signal-to-noise ratio, and yields image information that is limited only by the statistical fluctuation present in all photon data.

The only disadvantages of current CCD cameras are their relatively high cost and the low temporal resolution. Readout speed can be increased by either reducing the digital accuracy or reading a small portion of a CCD array (15). As with nearly all semiconductor products, one can expect performance to increase and cost to decrease. High-quality video-rate frame transfer CCDs are under construction. Kodak has recently announced a 1320 by 1035 chip that can read out data at 8 bits at ten frames per second.

Two aspects of the CCD relevant to biology deserve comment. First, the CCD has extraordinary sensitivity (33). It should be possible to fluorescently label cellular components and use the extreme sensitivity of the CCD to detect single molecular events. Second, the CCD provides image data with very high photometric (numerical) accuracy. The image data are now of sufficient quality

that meaningful computerized image processing can remove optical aberrations or out-of-focus information in 2-D or 3-D biological images and thus extend the image resolution to the diffraction limit. The enhanced resolution, especially in the z direction, can afford new insights into biological phenomena.

REFERENCES AND NOTES

1. D. A. Williams *et al.*, *Nature (London)* **318**, 558 (1985).
2. A. S. Waggoner, in *Applications of Fluorescence in the Biomedical Sciences*, D. L. Taylor, A. S. Waggoner, R. F. Murphy, F. Lanni, R. R. Birge, Eds. (Liss, New York, 1986), pp. 3–28.
3. J. E. Sulston *et al.*, *Dev. Biol.* **100**, 64 (1983).
4. D. A. Agard and J. W. Sedat, *Nature (London)* **302**, 676 (1983).
5. D. A. Agard, *Annu. Rev. Biophys. Bioeng.* **13**, 191 (1984).
6. Y. Gruenbaum *et al.*, *J. Cell Sci.* (suppl. 1), 223 (1984).
7. D. Mathog, M. Hochstrasser *et al.*, *Nature (London)* **308**, 414 (1984).
8. M. Hochstrasser *et al.*, *J. Cell Biol.* **102**, 112 (1986).
9. D. Mathog, M. Hochstrasser, J. W. Sedat, *J. Microsc. (Oxford)* **137**, 241 (1985).
10. D. Mathog, *ibid.*, p. 253.
11. C. R. Kitchin, *Astrophysical Techniques* (Hilger, Bristol, U.K., 1984), pp. 6–31.
12. M. M. Blouke, J. R. Janesick, J. E. Hall, M. W. Cowens, P. J. May, *Opt. Eng.* **22**, 607 (1983); J. Kristian and M. Blouke, *Sci. Am.* **247**, 66 (October 1982).
13. J. A. Connor, *Proc. Natl. Acad. Sci. U.S.A.* **83**, 6179 (1986).
14. Although CCDs show high quantum efficiency over the range of 500 to 1000 nm, the electrode structure of most CCDs limits blue sensitivity. To obtain the extended blue sensitivity often required for fluorescence microscopy, the chip usually must be thinned and illuminated from the back so that the light does not first go through the electrodes on the front surface. Texas Instruments have designed CCDs by using what they call a "virtual phase" structure that greatly reduces the amount of electrode on the front surface of the chip. With this design, high sensitivity into the ultraviolet can be provided in front-illuminated chips.
15. Our CCD system can transfer data at 50,000 pixels/sec at 14 bit resolution (13 seconds for full 1024 by 640 image, faster for subregions). The readout time is proportional to the area to be read out and the digital resolution. Other versions of the controller are available that transfer data faster but at decreased digital resolution.
16. Because the set of exposure times are the same for all pixels, it is convenient to use the correlation coefficient as a figure of merit. Coefficients that were more than 5 SD from the mean correlation coefficient were considered problematic. For these data the mean \pm SD of the correlation coefficient was 0.99999 ± 0.00002 .
17. Linearity was tested on the microscope at the wavelength produced by mercury arc illumination with several Zeiss filters, including a 405-nm band pass (BP), a 450- to 490-nm BP, a 546-nm BP, and a 590-nm long-wavelength pass, and by also using fluorescent dyes, such as DAPI (emission maximum 450 nm), rhodamine (590 nm), and Texas Red (615 nm).
18. K. R. Castleman, *Digital Image Processing* (Prentice-Hall, Englewood Cliffs, NJ, 1979), pp. 139–189.
19. Correction files are routinely made by using pixel-by-pixel linear regression analysis in a similar manner to that described but as a function of the average intensity of each image instead of exposure time to avoid problems associated with fluorescent dye fading.
20. K. Morikawa and M. Yanagida, *J. Biochem. (Tokyo)* **89**, 693 (1981); S. Matsumoto, K. Morikawa, M. Yanagida, *J. Mol. Biol.* **152**, 501 (1981); M. Yanagida, Y. Hiraoka, I. Katsura, *Cold Spring Harbor Symp. Quant. Biol.* **47**, 177 (1983).
21. H. H. Hopkins, *Proc. R. Soc. London A231*, 91 (1955).
22. P. A. Stokseth, *J. Opt. Soc. Am.* **59**, 1314 (1969).
23. The following objective lenses were tested: Leitz 63 \times (NA = 1.4) Planapo oil lens, Zeiss Neofluar 100 \times (NA = 1.3) oil lens, Zeiss Axiomat Planapo 100 \times (NA = 1.3) oil lens (for polarized light), Zeiss Planapo 63 \times (NA = 1.2) water lens (cover slip-free), Zeiss Planapo 40 \times (NA = 1.0) oil lens (with iris), and Zeiss Plan-Neofluar 40 \times (NA = 0.9) oil-glycerol-water lens (with correction collar).
24. S. Inoué, personal communication; M. Cagnet, M. Francon, J. C. Thierri, *Atlas of Optical Phenomena* (Springer-Verlag/Prentice-Hall, Englewood Cliffs, NJ, 1962).
25. Y. Hiraoka, J. W. Sedat, D. A. Agard, unpublished data.
26. D. A. Agard, R. A. Steinberg, R. M. Stroud, *Anal. Biochem.* **111**, 257 (1981).
27. A. S. Belmont, J. W. Sedat, D. A. Agard, unpublished data.
28. T. J. Mitchison and J. W. Sedat, *Dev. Biol.* **99**, 261 (1983).
29. K. Umeson, Y. Hiraoka, T. Toda, M. Yanagida, *Curr. Genet.* **7**, 123 (1983).
30. Y. Hiraoka, T. Toda, M. Yanagida, *Cell* **39**, 349 (1984).
31. S. Inoué, *Video Microscopy* (Plenum, New York, 1986).
32. R. D. Allen, *Annu. Rev. Biophys. Chem.* **14**, 265 (1985).
33. Astronomers have shown that it is possible to image stellar galaxies (27th magnitude) that correspond to photon fluxes of 2 photons per second with a 4-meter telescope. See J. A. Tyson, *Topical Meeting on Quantum-Limited Imaging and Image Processing* (Optical Society of America, Washington, DC, 1986), pp. 12–15.
34. We thank R. Akins, Photometrics Ltd. (Tucson, AZ), for helpful discussions, S. Inoué for helpful discussion on optical phenomena and comments on the manuscript, M. Hall for *S. cerevisiae* cells, H. Selick for bacteriophage T4 DNA, and E. Blackburn, M. Rykowski, A. Belmont, and B. Alberts for critical reading of the manuscript. Supported in part by NIH GM25101-09 and NIH GM32803-03 to J.W.S. and NIH GM31627 to D.A.A. and by Howard Hughes Medical Institute to J.W.S. and D.A.A. D.A.A. was also supported by a grant from the National Cancer Research Foundation, and by Searle Scholars and NSF Presidential Young Investigator Programs. Y.H. was supported by Damon Runyon-Walter Winchell Cancer Fund Fellowship DRG903.